Vibration compensation of an atom gravimeter

Aopeng Xu (许翱鹏)[1], Delong Kong (孔德龙)[1], Zhijie Fu (付志杰)[1], Zhaoying Wang (王兆英)[1,*], and Qiang Lin (林 强)[2,]**

[1]*Institute of Optics, Department of Physics, Zhejiang University, Hangzhou 310027, China*
[2]*Center for Optics and Optoelectronics Research, College of Science, Zhejiang University of Technology, Hangzhou 310014, China*
**Corresponding author: zhaoyingwang@zju.edu.cn; **corresponding author: qlin@zju.edu.cn*
Received January 7, 2019; accepted March 28, 2019; posted online June 25, 2019

For most atom interferometers, the vibration isolation unit is applied to reduce vibration noise. In our experiment, instead of isolation, the vibration signals are monitored, and combining with the sensitive function, the compensation phase shift for the atom interferometer is obtained. We focus on the correction over a wide spectrum rather than on "monochromatic" frequencies. The sensitivity of the atom gravimeter can be upgraded by a factor of more than two. Furthermore, we demonstrate that the atom interferometer can still produce a good measurement result without passive vibration isolation in extremely noisy environments by using vibration compensation.

OCIS codes: 020.3320, 000.2780, 270.5570.
doi: 10.3788/COL201917.070201.

The cold atom interferometer has been implemented since 1991[1] and developed rapidly in the last 20 years. It is very useful in both fundamental physics[2–6] and technical applications[7–14]. The gravimeter based on atom interference is an effective instrument to measure the small changes of the gravity field[15–18]. According to the equivalence principle, it is impossible to distinguish the acceleration of gravity from accelerations of the reference frame of measurement. Therefore, an atom interferometer is very sensitive to the vibration of the instrument. Many experimental results have shown that for an atom interferometer, precision measurement of gravity cannot be performed without any suppression of vibration noise[19,20]. To reduce the noise of vibration, most of the experimental groups used passive[16,20,21] or active vibration isolation units[10,19,22–24]. Passive isolation alone reduces the acceleration error signal by a factor of 30 above 10 Hz[24], and the acceleration error signal is reduced by an additional factor of up to more than 500 from 0.1 to 10 Hz with active isolation[22]. Vibration compensation is also a commonly used method to restrain vibration noise. There are two kinds of vibration compensation: the first one is post-correction, and the second one is real time compensation. Based on the passive vibration isolation platform, the LNE-SYRTE experimental group used vibration compensation and obtained good results[25–27]. Most of the results are obtained by exciting the experiment at a well-defined frequency. In this Letter, we present a method that monitors the vibration signals to correct the measurement results. We focused on the correction over a wide spectrum rather than on "monochromatic" frequencies.

The principle of the atom gravimeter has been well-described[1,19]. The apparatus of our atom gravimeter has been previously described in detail in another Letter[21]. But in this Letter, under the retro-reflection mirror, we do not place an isolation platform as in Ref. [21], instead we replaced it with a seismometer, as seen in Fig. 1. The stimulated Raman transitions manipulate the atom population of the two ground hyperfine sublevels $^5S_{1/2}$, $F=1$ and $^5S_{1/2}$, $F=2$ of the cooled ^{87}Rb atoms. The Raman beam is composed of two beams with wave vectors $\boldsymbol{k}_1$ and $\boldsymbol{k}_2$. The stimulated Raman transition of the atom gravimeter is the combination of $\pi/2-\pi-\pi/2$ Raman pulses with the duration $\tau-2\tau-\tau$, where τ is the action time of a $\pi/2$ Raman pulse. The three pulses are separated by an interval time T.

Assuming all of the ^{87}Rb atoms are in the initial state of $F=2$, the interference fringes can be observed, and the atom probability in the $F=1$ state can be written as[16]

$$P_{2\to1}=\frac{1}{2}\{1-\cos[(\boldsymbol{k}_{\text{eff}}\cdot\boldsymbol{g}-\alpha)\,T^2+\Delta\phi]\},\qquad(1)$$

where $\boldsymbol{k}_{\text{eff}}=\boldsymbol{k}_1-\boldsymbol{k}_2$ is the effective wave vector of Raman beams, α is the chirp rate of the effective Raman laser frequency used to compensate the Doppler shift due to gravity $\boldsymbol{g}$, and $\Delta\phi$ can be considered as a measurement error.

In our experiment, the Raman beams consist of two extended cavity diode lasers; the frequency difference of

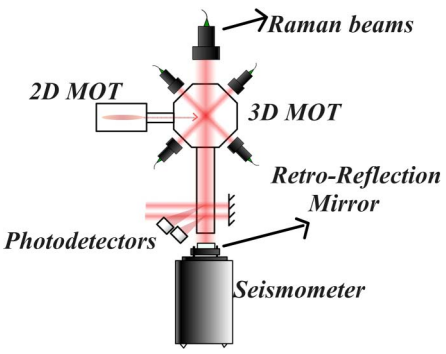

Fig. 1. Schematic diagram of our atom gravimeter.

the lasers is phase locked onto a microwave reference source[28]. There are many factors affecting $\Delta\phi$, such as the noise of the reference source and the vibration of the retro-reflection mirror[19]. According to the equivalence principle, the accelerations of the reference frame of the Raman laser field will result in phase shifts that are indistinguishable from the gravity value. The phase noise of Raman beams caused by the reference source can be calculated[29]. If $T = 50$ ms and $\tau = 8$ μs, the contribution of the Raman phase noise relative to the atom interferometer can be calculated to be about 41 mrad.

In addition to the phase noise of Raman beams, the vibration of the mirror reflecting the Raman beams can also affect $\Delta\phi$ and become another major noise source. In order to evaluate the vibration of the retro-reflection mirror, we fixed the mirror at the top of the seismometer, which was used to collect the vibration signals of the mirror. The sensitive seismometer (Guralp CMG-3ESP) provides us with hardware to measure the displacement of the mirror. In order to simulate the different vibration conditions, we also use a high-power speaker to produce a single frequency vibration. It would be a useful tool to measure the frequency response of the seismometer.

The interferometer phase shift induced by the vibration of the mirror can be written as[29]

$$\Delta\phi_v = k_{\text{eff}} \int_{-T}^{T} g(t)v(t)\mathrm{d}t, \tag{2}$$

where $v(t)$ is the velocity of the mirror, and $g(t)$ is the sensitivity function of the interferometer. If we choose the center of the sequence of three Raman laser pulses as the original time, $g(t)$ can be written as

$$g(t) = \begin{cases} 0, & \text{for } t < -T - 2\tau \\ -\sin[\Omega_R(t + T + 2\tau)], & \text{for } -T - 2\tau \le t < -T - \tau \\ -1, & \text{for } -T - \tau \le t < -\tau \\ \sin[\Omega_R(t + T + 2\tau)], & \text{for } -\tau \le t < \tau \\ 1, & \text{for } \tau \le t < T + \tau \\ -\sin[\Omega_R(t - T - 2\tau)], & \text{for } T + \tau \le t < T + 2\tau \\ 0, & \text{for } T + 2\tau < t \end{cases}, \tag{3}$$

where Ω_R is the Raman Rabi frequency. Then, if we acquire the mirror velocity, we can calculate the vibration correction phase $\Delta\phi_v$ by using Eq. (2).

After obtaining the vibration correction phase of the mirror, we would like to learn the variance of the vibration phase $\sigma^2_{\Delta\phi}$, which is an intuitive standard for evaluating phase stability. It can be written as

$$\sigma^2_{\Delta\phi} = \int_{-\infty}^{+\infty} S_\phi(\omega)|H(\omega)|^2\mathrm{d}\omega, \tag{4}$$

where $S_\phi(\omega)$ is the power spectral density of the vibration phase, and $H(\omega)$ is the phase noise weighting function. The weighting function is given by $H(\omega) = \omega G(\omega)$, where $G(\omega)$ is the Fourier transform of the sensitivity function $g(t)$.

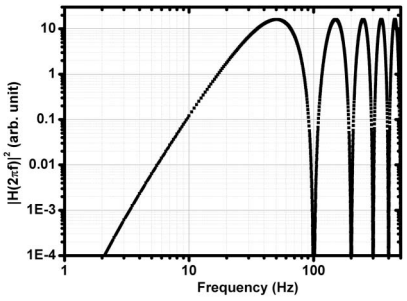

Fig. 2. Below 500 Hz, the weighting function for the vibration phase noise as a function of frequency.

The weighting function $|H(\omega)|^2$ versus the frequency f is shown in Fig. 2, while $T = 10$ ms and $\tau = 6$ μs. The weighting function can also be used to evaluate the degradation caused by the vibration of the mirror[29].

According to Eq. (2), we can calculate the phase shift $\Delta\phi_v$ due to the mirror vibration. If the mirror and seismometer are absolutely rigid connections, the vibration of the mirror and seismometer should be the same. In our experiment, the retro-reflection mirror is only fixed above the seismometer by a machine screw. So, there would be some difference between the seismometer measurements $v_s(t)$ and the actual vibration $v(t)$ of the mirror. Suppose $v_{\text{in}}(t)$ is the original vibration of the seismometer, $v_{\text{out}}(t)$ is the output of the seismometer. $V_{\text{in}}(s)$ and $V_{\text{out}}(s)$ are Laplacian variations of $v_{\text{in}}(t)$ and $v_{\text{out}}(t)$. The transfer function of the seismometer is $X(s) = V_{\text{out}}(s)/V_{\text{in}}(s)$. If the amplitude and phase transfer between the signal recorded by the seismometer and the real vibration of the seismometer are $A(f)$ and $\varphi(f)$, then the relationship between these parameters can be written as $A(f) = |X(2\pi jf)|$ and $\varphi(f) = \text{Arg}[X(2\pi jf)]$, where $j = \sqrt{-1}$. Suppose there is a single frequency vibration, the vibration of the mirror is given by

$$v(t) = B\sin(2\pi ft + C), \tag{5}$$

where B is the amplitude, and C is the initial phase. Then, the seismometer measurement's vibration can be written as

$$v_s(t) = A(f)B\sin[2\pi ft + C + \varphi(f)]. \tag{6}$$

The interferometer phase shift $\Delta\phi_v$ in Eq. (2) should be modified as

$$\begin{aligned} \Delta\phi_v &= k_{\text{eff}} \int_{-T}^{T} g(t)v(t)\mathrm{d}t \\ &= \frac{k_{\text{eff}}}{A(f)} \int_{-T}^{T} g(t)A(f)B\sin(2\pi ft + C)\mathrm{d}t \\ &= \frac{k_{\text{eff}}}{A(f)} \int_{-T-\Delta T}^{T-\Delta T} g(t + \Delta T)A(f)B \\ &\quad \times \sin[2\pi f(t + \Delta T) + C]\mathrm{d}t. \end{aligned} \tag{7}$$

When $2\pi f\Delta T = \varphi(f)$, Eq. (7) can be written as

$$\begin{aligned}\Delta\phi_v &= \frac{k_{\text{eff}}}{A(f)}\int_{-T-\Delta T}^{T-\Delta T} g(t+\Delta T)A(f)B \\ &\quad\times \sin[2\pi f(t+\Delta T)+C]\mathrm{d}t \\ &= \frac{k_{\text{eff}}}{A(f)}\int_{-T-\frac{\varphi(f)}{2\pi f}}^{T-\frac{\varphi(f)}{2\pi f}} g\left[t+\frac{\varphi(f)}{2\pi f}\right]v_s(t)\mathrm{d}t. \end{aligned} \tag{8}$$

In this case, the interferometer phase shift $\Delta\phi_v(f)$ depends on the transfer function $A(f)$, $\varphi(f)$, and sensor measurements $v_s(t)$.

Now, we would like to study the transfer function, which must be calibrated before the experiment. The most direct way to calibrate the transfer function is to fix the seismometer, mirror, and vibration source to a large isolation platform. When the vibration source generates a single frequency vibration, the signal of the seismometer is recorded, and the vibration of the mirror is measured by other reference measurements[30]. In our experiment, we can use the atom interferometer itself to calibrate the transfer function between the seismometer and the mirror.

In order to measure the transfer function for different frequencies, we must add a frequency-variable vibration to the system. To produce single frequency vibration, we use a high-power speaker, which is placed 0.3 m away from the center of the atom interferometer. It is very difficult to produce a single frequency vibration because of the frequency multiplier effect, especially for low frequency. In our experiment, we drive a 50 Hz sine wave source to the speaker, and the output vibration signal of the mirror is collected by the seismometer, as shown in Fig. 3. We can find that the collected signal is a deformed sine wave with 100 Hz frequency.

Fortunately, we can choose a proper T to reduce the contribution of the multiplier frequency to the gravimeter. For example, with $f = 50$ Hz, we can set the interval time $T = 10$ ms; then, we will have $H(50\text{ Hz}) = 16$ while $H(100\text{ Hz}) = 0$. Figure 4 shows the influence of different frequency vibrations on the atom interferometer. The power spectral density of vibration velocity is shown as the red line, with a frequency of 50 Hz. The weighting function $|H(2\pi f)|^2$ with the interval time $T = 10$ ms is shown as the grey dash. Under the influence of the weighting function, 100 Hz vibration does not affect the interferometer fringe, which is shown as the dark dot curve.

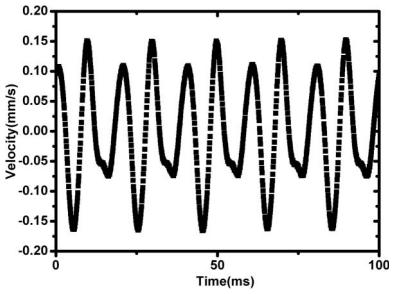

Fig. 3. 50 Hz vibration signal collected by the seismometer.

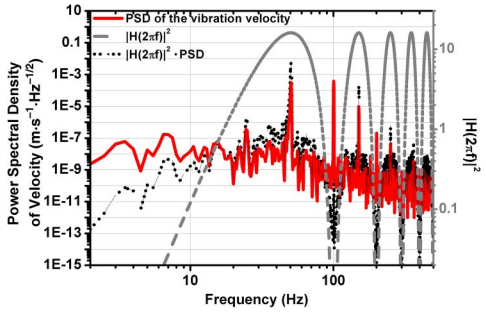

Fig. 4. Influence of different frequency vibrations on the atom interferometer.

Finally, we focus on the measurement of the transfer function. We use a high-power speaker to generate a single frequency vibration, using the seismometer to record the vibration signal at the same time. We measure the atom probability in the $F = 1$ state repeatedly, and the chirp rate of the effective Raman laser frequency is fixed at α_0. In the absence of noise, the atom probability would be a constant value. In our experiment, although the frequency and amplitude of the vibration were constant, the initial phase C is randomly distributed. For each measurement, the vibration phase shift $\Delta\phi_v(f)$ calculated according to Eq. (7) is random. Due to the effects of vibration, the probability will oscillate, satisfying the relationship of Eq. (2). Based on Eq. (8), if we calibrate correctly the transfer function $\varphi(f)$ and $A(f)$, we can calculate the vibration phase shift $\Delta\phi_v(f)$ and get a sinusoidal curve for the atom probability, which is shown as Fig. 5. If the transfer function $\varphi(f)$ is not correctly measured, the vibration phase $\Delta\phi_v(f)$ cannot be calculated correctly, and the relation between the atom population $P_{2\to1}$ and the vibration phase $\Delta\phi_v(f)$ will not become sinusoidal. We can set $\varphi(f)$ to a different value by scanning ΔT, and the value at which the sine fitting residual is the smallest reflects the true phase transfer function.

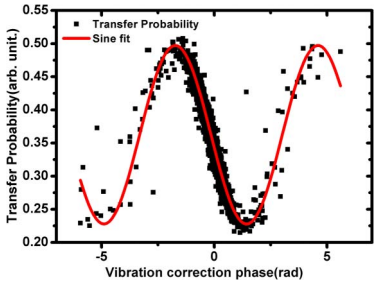

Fig. 5. After calibration of the transfer functions $A(50\text{ Hz})$ and $\varphi(50\text{ Hz})$, a sinusoidal curve is obtained. The black dot is the relationship between transfer probability and vibration correction phase; we use the seismometer to record the vibration and calculate the correction phase, and the transfer probability is measured by the atom interferometer. The red line is the sine fit.

The amplitude response of the transfer function $A(f)$ is related to the frequency of the sinusoidal curve.

After calibration of the transfer functions $A(f)$ and $\varphi(f)$, the transfer function can be written as

$$X(f) = A(f)e^{j\varphi(f)}. \tag{9}$$

Although we only measured the transfer function for a few specific frequencies, we can obtain a continuous transfer function of the whole spectrum using quadratic spline interpolation. The inverse fast Fourier transformation is performed on $1/X(f)$ to obtain the time domain function $x(t)$. Then, we can get the vibration of the mirror,

$$v(t) = x(t) * v_s(t), \tag{10}$$

where "$*$" indicates convolution.

The inversion algorithms have some limitations. Since $X(0\ \text{Hz}) = 0$, $1/X(f)$ is infinite, $f \approx 0$ Hz. Before we perform the inverse fast Fourier transform, the magnitude of $1/X(f)$ is directly regarded as zero when $f < f_s/200$. f_s is the sampling frequency of the vibration data acquisition, and $f_s = 1$ kHz in our system. If $f < 5$ Hz, $1/X(f) = 0$, and we cannot get to the corrected vibration signal. When $f > 200$ Hz, due to our measurement repetition time limitation, there will be less than five experiment data points in each vibration period; then, we cannot have high accuracy of the integral, which will affect the integral calculation of $\Delta\phi_v$. We can only study the transfer function for the frequency between 5 and 200 Hz in this Letter. Moreover, $v_s(t)$ must be a signal that is close to infinitely long in the time domain. In our experiments, the vibration signal at each point of the interference fringes was continuously acquired for 40 s.

Without considering the influence of the transfer function between the mirror and the seismometer, we could not get a good compensation result. Figure 6 shows the original fringes without vibration compensation, the compensation fringes without frequency response calibration, and the compensation fringes considering frequency response calibration. In Fig. 6(b), we can get an excellent interference fringe, shown as sinusoidal distribution, while the vibration frequency is 50 Hz. However, if we use the same amplitude and phase delay to compensate the fringe while the vibration frequency is 80 Hz, the fringe would not be distributed as a sinusoidal curve, as shown in Fig. 6(d). After the transfer function calibration, the results have clearly improved, as shown in Fig. 6(e).

The original data of atom interference is obtained and displayed as the dark square points in Fig. 7. There is no additional vibration. The interval time of the Raman pulses is $T = 60$ ms, and the chirp rate is $\Delta\alpha = \alpha +$ 25.10344 MHz. As shown in Fig. 7, the sinusoidal shape of the interference fringe is not significant. After the vibration compensation, the original data is modified as the green triangle points in Fig. 7, and the sinusoidal curve can be obtained and fitted as the red line.

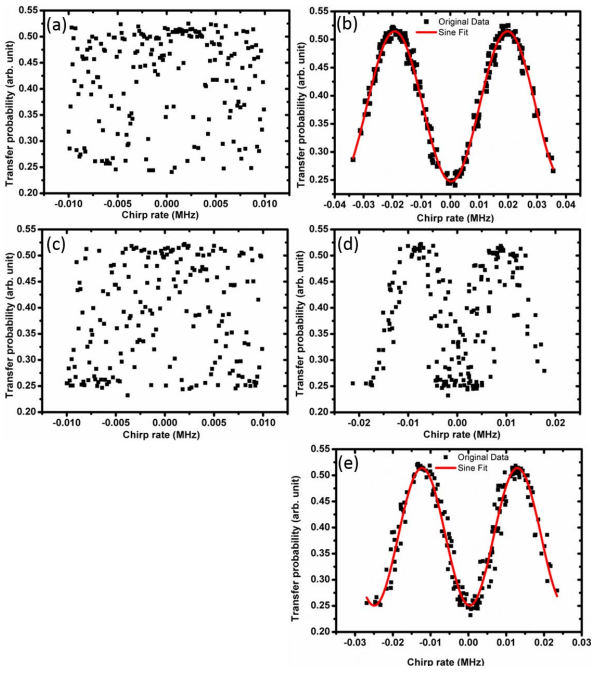

Fig. 6. Interference fringes in different vibration compensations. (a) The original fringe without vibration compensation while the vibration frequency is 50 Hz. (b) The fringe after vibration compensation while the vibration frequency is 50 Hz, $A(50\ \text{Hz}) = -1.299$ dB, and $\varphi(50\ \text{Hz}) = -64$ deg. (c) The original fringe without vibration compensation while the vibration frequency is 80 Hz. (d) The fringe after vibration compensation while the vibration frequency is 80 Hz, $A(80\ \text{Hz}) = -1.299$ dB, and $\varphi(80\ \text{Hz}) = -64$ deg. (e) The fringe after vibration compensation while the vibration frequency is 80 Hz, $A(80\ \text{Hz}) = -4.895$ dB, and $\varphi(80\ \text{Hz}) = -143.2$ deg.

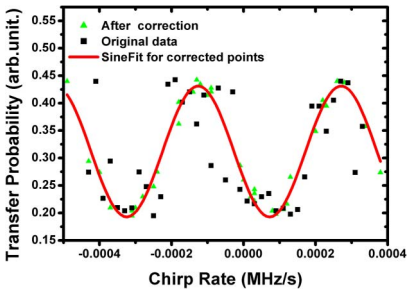

Fig. 7. Atom interference fringe can be optimized by using vibration compensation.

Using vibration compensation, the atom interferometer can still produce a good measurement result without any passive vibration isolation in some extremely noisy environments, as shown in Fig. 8. We use the speaker to generate a vibration with a frequency of 50 Hz. The interval time of the Raman pulses is set as 10 ms. The black dots are the original experimental data. The scan range is only 0.02 MHz/s, which is converted to the phase of less than π rad. After vibration compensation, the original data is modified as the green points in Fig. 8. We find that the

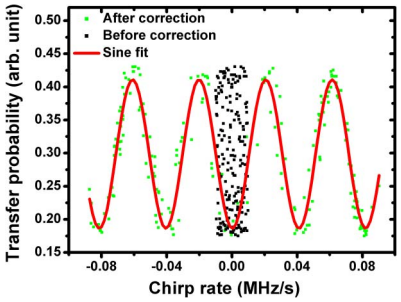

Fig. 8. Atom interference fringe in an extremely noisy environment. The black dot is the data before vibration compensation, the green dot is the data after vibration compensation, and the red line is the sine fit of the green dot.

vibration compensation method can compensate the phase caused by vibration noise greater than 4π rad.

We also evaluate the feasibility of the vibration compensation method by Allan standard deviation for long term stability. When $T = 60$ ms, a resolution of 32 μGal is obtained after an integration time of 25.6 s, as Fig. 9 shows. As a comparison, we used the passive isolation platform and the vibration compensation method to measure the gravity. Firstly, we simulate one lower vibration surrounding without the speaker. Figure 9 shows the comparison of Allan standard deviation for the passive vibration isolation and the vibration compensation. When the speaker is not working, only the environment vibration exists, and the passive vibration isolation method obtains the best result. The Allan standard deviation of the vibration compensation is approximately 1.5 times the result of the passive vibration isolation, but there is still an obvious improvement compared to no vibration suppression.

We also simulate one strong vibration surrounding. As we know, when the environment vibration is large, the passive vibration isolation cannot get good results[24]. However, the vibration compensation can compensate the vibration phase greater than 4π rad, as shown in Fig. 8. Therefore, the vibration compensation will have more advantages when the environmental vibration is large. We set the speaker's vibration frequency as 50 Hz, the interval time of Raman pulses $T = 50$ ms, and the sampling time is 25.6 s. We measure the gravity for different vibration amplitudes, as shown in Fig. 10. From Fig. 10, we can see that when the peak-to-peak vibration amplitude is

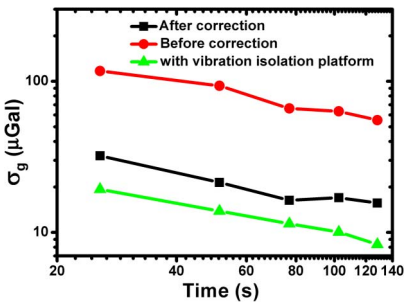

Fig. 9. Allan standard deviation of three different situations.

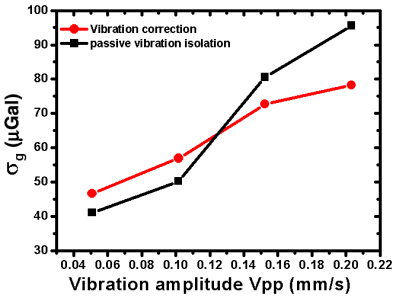

Fig. 10. Gravity measurement versus the different vibration amplitudes.

greater than 0.15 mm/s, the results of the vibration compensation are better than the passive vibration isolation.

Furthermore, we compare the performance of the vibration compensation method at different frequencies. Figure 11 is a comparison of gravity measurements before and after vibration compensation at different vibration frequencies, while $T = 50$ ms, and the peak-to-peak vibration amplitude is 0.20 mm/s. As shown in Fig. 11, the vibration compensation can obtain good results for the frequency between 50 and 170 Hz. Due to the limitation of the power speaker, we cannot produce a vibration with $f < 50$ Hz. We have to say that we can only correctly invert the real vibration signal within a certain frequency range.

In conclusion, we have introduced our vibration compensation method. At different vibration frequencies and vibration amplitudes, our vibration compensation method can get good results in some special conditions. The vibration compensation method can compensate the phase caused by vibration noise greater than 4π rad. Since a seismometer collected vibration signal does not reflect the true vibration of a Raman mirror, we measured the transfer function between the seismometer and the mirror to invert the real vibration signal. For our experimental setup, we can compensate for the vibration phase with the vibration frequency from 50 to 170 Hz. For vibration below 50 Hz, the passive or active vibration isolation can be used to restrain the vibration noise of the atom interference gravimeter. Due to the space limitation in our laboratory, we cannot use the passive vibration isolation platform and the seismometer at the same time. In the

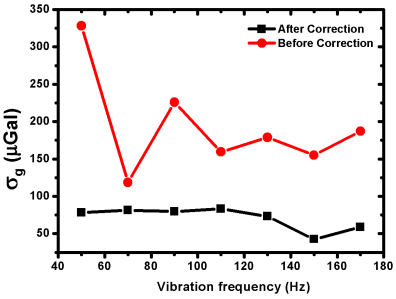

Fig. 11. Gravity measurement result at different vibration frequencies.

future, our laboratory can be re-planned, and it would have enough space to accommodate both the passive vibration isolation platform and the vibration compensation devices. The passive vibration isolation platform can be used to restrain the vibration of most frequencies, and the vibration compensation method can be used to compensate large-amplitude vibrations of a specific frequency; then, the vibration noise of the atom interference gravimeter will be further restrained.

This work was supported by the National Key Research and Development Program of China (No. 2017YFC0601602) and the Fundamental Research Funds for the Central Universities, China (No. 2018FZA3005).

References

1. M. Kasevich and S. Chu, Phys. Rev. Lett. **67**, 181 (1991).
2. J. B. Fixler, G. T. Foster, J. M. McGuirk, and M. A. Kasevich, Science **315**, 74 (2007).
3. S. Dimopoulos, P. W. Graham, J. M. Hogan, and M. A. Kasevich, Phys. Rev. Lett. **98**, 111102 (2007).
4. A. Bertoldi, G. Lamporesi, L. Cacciapuoti, M. de Angelis, M. Fattori, T. Petelski, A. Peters, M. Prevedelli, J. Stuhler, and G. M. Tino, Eur. Phys. J. D **40**, 271 (2006).
5. M. A. Hohensee, S. Chu, A. Peters, and H. Müller, Phys. Rev. Lett. **106**, 151102 (2011).
6. P. Cladé, E. Mirandes, M. Cadoret, S. Guellati- Khélifa, C. Schwob, F. Nez, L. Julien, and F. Biraben, Phys. Rev. Lett. **96**, 033001 (2006).
7. T. L. Gustavson, P. Bouyer, and M. A. Kasevich, Phys. Rev. Lett. **78**, 2046 (1997).
8. S. N. Lea, A. Clairon, C. Salomon, P. Laurent, B. Lounis, J. Reichel, A. Nadir, and G. Santarelli, Phys. Scripta. **T51**, 78 (1994).
9. Y. Bidel, O. Carraz, R. Charrière, M. Cadoret, N. Zahzam, and A. Bresson, Appl. Phys. Lett. **102**, 144107 (2013).
10. M. Hauth, C. Freier, V. Schkolnik, A. Senger, M. Schmidt, and A. Peters, Appl. Phys. B **113**, 49 (2013).
11. C. Y. Shi, R. Wei, Z. C. Zhou, D. S. Lu, T. Li, and Y. Z. Wang, Chin. Opt. Lett. **8**, 549 (2010).
12. Z. X. Xiong, Y. Long, H. X. Xiao, X. Zhang, L. X. He, and B. L. Lu, Chin. Opt. Lett. **9**, 041406 (2011).
13. X. S. Yan, C. F. Wu, J. Q. Huang, J. W. Zhang, and L. J. Wang, Chin. Opt. Lett. **15**, 040202 (2017).
14. Y. N. Wang, Y. L. Meng, J. Y. Wan, L. Xiao, M. Y. Yu, X. Wang, X. C. Ouyang, H. D. Cheng, and L. Liu, Chin. Opt. Lett. **16**, 070201 (2018).
15. Z. J. Fu, Q. Y. Wang, Z. Y. Wang, B. Wu, B. Cheng, and Q. Lin, Chin. Opt. Lett. **17**, 011204 (2019).
16. M. Kasevich and S. Chu, Appl. Phys. B **54**, 321 (1992).
17. M. J. Snadden, J. M. McGuirk, P. Bouyer, K. G. Haritos, and M. A. Kasevich, Phys. Rev. Lett. **81**, 971 (1998).
18. Y. P. Wang, J. Q. Zhong, X. Chen, R. B. Li, D. W. Li, L. Zhu, H. W. Song, J. Wang, and M. S. Zhan, Opt. Commun. **375**, 34 (2016).
19. A. Peters, K. Y. Chung, and S. Chu, Metrologia **38**, 25 (2001).
20. Q. Y. Wang, Z. Y. Wang, Z. J. Fu, and Q. Lin, Chin. Phys. B **25**, 123701 (2016).
21. B. Wu, Z. Wang, B. Cheng, Q. Wang, A. Xu, and Q. Lin, Metrologia **51**, 452 (2014).
22. M. K. Zhou, X. Xiong, L. L. Chen, and Z. K. Hu, Rev. Sci. Instrum. **86**, 046108 (2015).
23. M. K. Zhou, Z. K. Hu, X. C. Duan, B. L. Sun, L. L. Chen, Q. Z. Zhang, and J. Luo, Phys. Rev. A. **86**, 043630 (2012).
24. J. M. Hensley, A. Peters, and S. Chu, Rev. Sci. Instrum. **70**, 2735 (1999).
25. J. Le Gouët, T. E. Mehlstäubler, J. Kim, and F. P. Dos Santos, Appl. Phys. B **92**, 133 (2008).
26. B. Fang, I. Dutta, P. Gillot, D. Savoie, J. Lautier, B. Cheng, C. L. Garrido Alzar, R. Geiger, S. Merlet, F. P. Dos Santos, and A. Landragin, J. Phys.: Conf. Series **723**, 012049 (2016).
27. S. Merlet, J. Le Gouët, Q. Bodart, A. Clairon, A. Landragin, F. P. Dos Santos, and P. Rouchon, Metrologia **46**, 87 (2001).
28. X. L. Wang, T. J. Tao, B. Cheng, B. Wu, Y. F. Xu, Z. Y. Wang, and Q. Lin, Chin. Phys. Lett. **28**, 084214 (2011).
29. P. Cheinet, B. Canuel, F. P. Dos Santos, A. Gauguet, F. Leduc, and A. Landragin, IEEE. Trans. Instrum. Meas. **57**, 1141 (2008).
30. J. Le Gouët, "Etude des performances d'un gravimètre atomique absolu: sensibilité limite et exactitude préliminaire," Ph.D. Thesis (Université Paris Sud-Paris XI, 2008).